Hyperfine Interact (2016) 237:87
DOI 10.1007/s10751-016-1275-8

Stiffness, resilience, compressibility

Atomic scale force spectroscopy of biomolecules

Bogdan M. Leu[1] · **J. Timothy Sage**[2]

Abstract The flexibility of a protein is an important component of its functionality. We use nuclear resonance vibrational spectroscopy (NRVS) to quantify the flexibility of the heme iron environment in the electron-carrying protein cytochrome *c* by measuring the stiffness and the resilience. These quantities are sensitive to structural differences between the active sites of different proteins, as illustrated by a comparative analysis with myoglobin. The elasticity of the entire protein, on the other hand, can be probed quantitatively from NRVS and high energy-resolution inelastic X-ray scattering (IXS) measurements, an approach that we used to extract the bulk modulus of cytochrome *c*.

Keywords Nuclear resonance vibrational spectroscopy · Heme proteins · Flexibility

1 Introduction

Structure, dynamics, and functionality are three properties of a protein, with the protein flexibility being involved in all of them: on the one hand, it is affected by the structure, while, on

This article is part of the Topical Collection on *Proceedings of the International Conference on the Applications of the Mössbauer Effect (ICAME 2015), Hamburg, Germany, 13–18 September 2015*

We acknowledge generous financial support from a National Science Foundation award CHE-1026369. Use of the Advanced Photon Source, an Office of Science User Facility operated for the U.S. Department of Energy (DOE) Office of Science by Argonne National Laboratory, was supported by the U.S. DOE under Contract No. DE-AC02-06CH11357.

✉ J. Timothy Sage
jtsage@neu.edu

[1] Advanced Photon Source, Argonne National Laboratory, Argonne, IL 60439, USA

[2] Department of Physics and Center for Interdisciplinary Research on Complex Systems, Northeastern University, Boston, MA 02115, USA

Published online: 30 March 2016

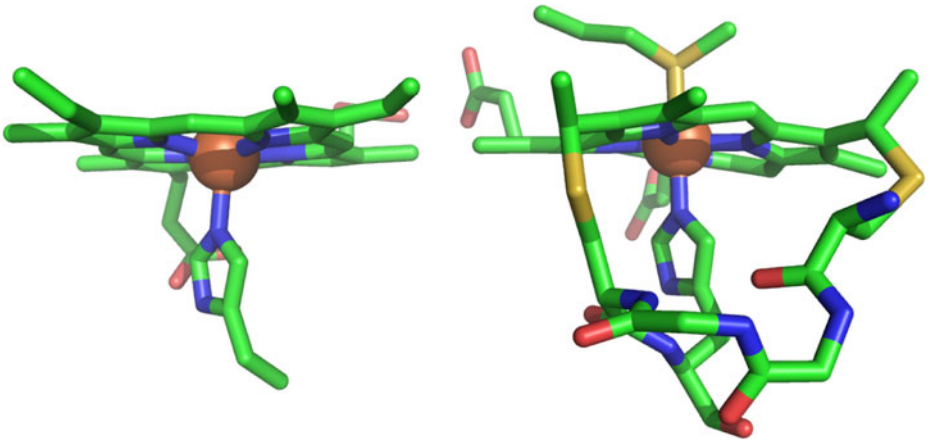

Fig. 1 Structure of the heme group in the active sites of deoxyMb (*left*) and Fe(III) cyt *c* (*right*). Both views are from the edge of the approximately planar heme group, emphasizing the covalent connections with the protein. An imidazole ring from a histidine residue below the heme ligates the Fe (depicted as an orange sphere) in both proteins. Fe ligation by the sulfur atom of a methionine residue located above the heme and covalent links between cysteine residues to the vinyl groups at the edge of the heme increase the connectivity to the protein in cyt *c*

the other hand, it influences the dynamics and the function. Our main experimental tool in this work is nuclear resonance vibrational spectroscopy (NRVS; also called nuclear inelastic scattering, NIS, or nuclear resonance inelastic X-ray scattering, NRIXS), a technique in which the signal is due only to the targeted Mössbauer isotope, with no contribution from other (non-resonant) atoms. Due to this remarkable site-selectivity, NRVS has emerged as a powerful method for probing specific iron-containing sites in molecules with extremely complex structures, such as proteins and enzymes. NRVS provided answers beyond the reach of protein crystallography and traditional spectroscopic techniques (resonance Raman and infrared) to outstanding questions related to the structure, dynamics, and functionality of heme proteins [1–4], iron-sulfur proteins [5–8], and other nonheme iron enzymes [9–11].

In the molecular sciences, conventional applications of vibrational spectroscopy emphasize the interpretation of individual frequencies as structural markers. In favorable cases, vibrational frequencies can be calibrated as highly sensitive probes of covalent bond lengths or local electric fields [12, 13]. However, quantitative interpretation of absolute spectral intensities remains challenging. Moreover, spectral congestion can inhibit the identification and assignment of individual frequencies, especially in complex systems such as biomolecules.

Here, we use the iron partial phonon density of states yielded by NRVS to calculate the *stiffness* (an effective force constant of the iron environment) and the *resilience* (a measure of the iron mean square displacement temperature-dependence) for cytochrome *c* (cyt *c*) and deoxymyoglobin (deoxyMb) and discuss them in terms of structural differences between the active sites of the two proteins (Fig. 1). Furthermore, we combine NRVS and inelastic X-ray scattering (IXS) results to calculate the bulk modulus of oxidized cyt *c*. Stiffness, resilience, and compressibility quantitatively capture important aspects of biomolecular structure and flexibility without requiring assignment of individual frequencies.

2 Experimental

Nuclear resonance vibrational spectroscopy (NRVS) NRVS [14–16] measures the vibrations of a Mössbauer nucleus (^{57}Fe in this study). This type of experiment requires the highly brilliant X-rays available at third-generation synchrotron facilities [17]. All NRVS experiments were carried out at the Advanced Photon Source, Argonne National Laboratory, beamline 3-ID-D. The energy of the incident photons was tuned around 14.4 keV, corresponding to a nuclear resonance of the ^{57}Fe isotope, with a bandpass around 1 meV. Direct fluorescent decay at 14.4 keV and internal conversion, followed by fluorescence of the ionized iron at 6.4 keV, contribute to the deexcitation of the ^{57}Fe nucleus. Both 14.4 keV and 6.4 keV photons, emitted with a delay on the order of the 141 ns excited state lifetime, contribute to the observed NRVS signal, while the background signal from electronically scattered photons is nearly coincident with the incident X-ray pulse and excluded from the experimental signal.

Normalization of the first moment of the measured signal according to Lipkin's sum rules [18] produces the excitation probability $S(E)$ and, upon further data analysis [19], the partial phonon density of states $D(E)$. Several quantities can be readily extracted from $S(E)$ and $D(E)$ [20]. Therefore, NRVS provides extensive quantitative information on the targeted isotope (frequencies, amplitudes, and directions) and its environment.

Inelastic X-ray scattering (IXS) The high energy-resolution inelastic X-ray scattering technique [21, 22] measures phonon dispersion curves in single crystals and probes collective excitations in disordered systems, including biological molecules [23–25]. IXS is a "photon-in/photon-out" technique that measures the dynamic structure factor with meV resolution at momentum transfers Q above 1 nm^{-1}. From the $E - Q$ dependence (E is the transferred energy), the longitudinal sound velocity v_L is extracted according to

$$E = \hbar v_L Q. \tag{1}$$

The experiment was carried out at the Advanced Photon Source, Argonne National Laboratory, beamline 3-ID-C [26], with a working energy of 21.7 keV and an energy resolution of $\approx$ 2.4 meV.

Enrichment of myoglobin and cytochrome *c* with the ^{57}Fe isotope Established methods [27] were used for the removal of the heme from horse heart myoglobin (Mb) and the replacement with ^{57}Fe-enriched heme. This approach, however, is not suitable for cyt *c* due to the additional covalent links between the heme and the protein (Fig. 1). As described in detail elsewhere [28], either hydrogen fluoride or, in a milder but less efficient procedure, a ferrous sulfate–hydrochloric acid solution, were used to extract the natural abundance iron from the covalently attached heme. The resulting porphyrin cyt *c* incorporates ^{57}Fe upon equilibration with isotopically enriched ferrous acetate, and the structural integrity of the reconstituted protein was confirmed spectroscopically for each procedure [28].

3 Results and discussion

The upper traces in Fig. 2 show the experimentally determined vibrational densities of states (VDOS) for Fe(II) cyt *c*, Fe(III) cyt *c*, and deoxyMb. The frequency ranges ($E = hc\bar{\nu}$, 1 meV $\approx$ 8 cm^{-1}) of the dominant features in these spectra (200 $-$ 300 cm^{-1} for deoxyMb, 300 $-$ 400 cm^{-1} for cyt *c*) reflect structural differences beteen the two proteins [29] (longer

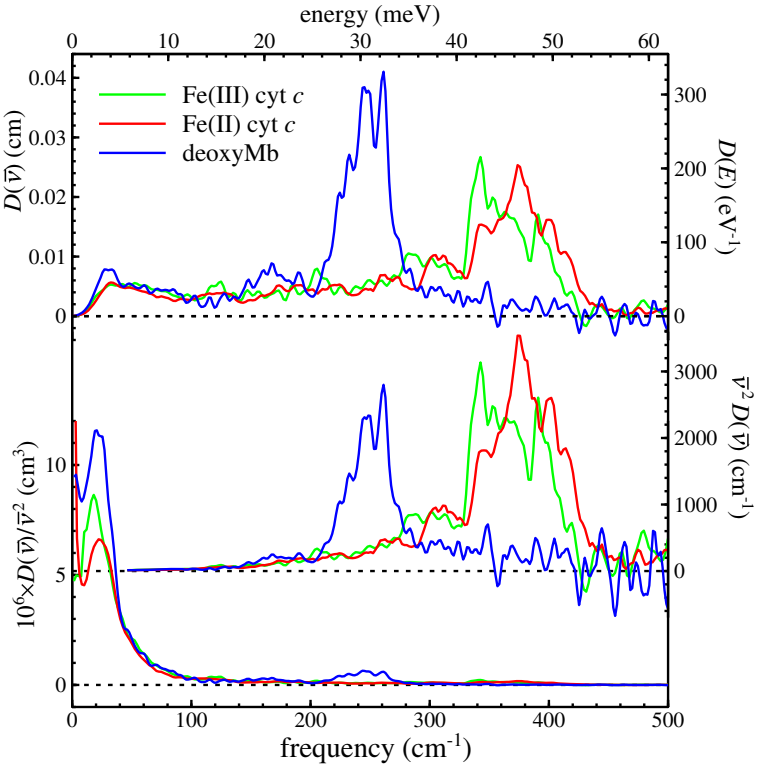

Fig. 2 Vibrational densities of states (VDOS) of the Fe atom in Fe(II) cyt *c*, Fe(III) cyt *c*, and deoxyMb. The upper traces compare the actual VDOS $D(\bar{\nu})$. Multiplication or division by a factor $\bar{\nu}^2$ in the middle and lower traces emphasizes the frequency regions that contribute to determining the stiffness (2) and resilience (4), respectively

Fe−N_{pyr} bonds in deoxyMb with respect to cyt *c* and shorter Fe−S(Met80) bond in Fe(II) cyt *c* with respect to Fe(III) cyt *c*).

Stiffness From the Fe VDOS one can extract the *stiffness* of the iron environment, an effective force constant [18]

$$k_s = m_{Fe}\left\langle \omega^2 \right\rangle = \frac{1}{3} m_{Fe}\,(2\pi c)^2 \int_0^\infty \bar{\nu}^2 D(\bar{\nu}) d\bar{\nu} \tag{2}$$

that measures the strength of the nearest-neighbor interactions with iron.

Inspection of the middle traces in Fig. 2 reveals that the modes corresponding to the dominant features in the VDOS ($200-300\ \mathrm{cm}^{-1}$ for deoxyMb, $300-400\ \mathrm{cm}^{-1}$ for cyt *c*) make the most important contribution to the integrand of (2) and thus to the stiffness. These values reflect structural differences among the three proteins investigated, demonstrating the sensitivity of stiffness to variations in the Fe-ligand bond lengths (Table 1). The sensitivity of the stiffness to small changes in Fe-S bond length in cyt *c* is particularly remarkable, because individual Fe-ligand stretching frequencies are experimentally unresolved in the VDOS.

Table 1 Effective force constants determined from the experimental vibrational density of states of heme iron, with associated structural and electronic properties

	Force constant (pN/pm)		Bond length (pm)			Iron	Heme
	Stiffness	Resilience	Fe—L_5	Fe—L_6	Fe—L_{eq}	spin	connectivity
Fe(II) cyt *c*	322 ± 17	32.6 ± 1.5	200 ± 2	229 ± 2	199 ± 2	0	4
Fe(III) cyt *c*	284 ± 17	28.3	198 ± 2	233 ± 2	198 ± 2	1/2	4
deoxyMb	190 ± 20	21.1 ± 1.3	220 ± 2		205 ± 2	2	1
Fe(OEP)(Cl)	196 ± 6	15.4 ± 0.5	223.1		206.5	5/2	0

The equatorial ligands (L_{eq}) of the iron are the four pyrrole nitrogens of the heme in each case. The fifth axial ligand (L_5) is the nitrogen of a histidine residue for each of the proteins and chloride for Fe(OEP)(Cl). In cytochrome *c*, Fe is additionally ligated by the sulfur atom of a methionine (L_6)

The improved NRVS signal typically available for small molecules is enabling more systematic exploration of how the stiffness responds to coordination changes (Table 2). Although chloride complexes of a series of Fe porphyrins [porphine (P), octaethylporphyrin (OEP), and protoporphyrin IX (PPIX)] exhibit significant variations in the observed VDOS [30], the stiffnesses are indistinguishable within experimental uncertainty (Tables 1 and 2). This suggests that the stiffness appropriately averages over detailed variations in the VDOS to extract a nearly invariant measure of the nearest neighbor interactions with the Fe. Similarly, the stiffness determined for the imidazole-ligated Fe porphyrin Fe(TPP)(2-MeHIm) (Table 2), which mimics the coordination of the heme Fe in deoxyMb, exhibits a stiffness that is experimentally indistinguishable from that found for deoxyMb (Table 1). On the other hand, the significantly reduced stiffness observed upon deprotonation of the imidazole ligand (Table 2) indicates that the stiffness is senstive to subtle changes in Fe ligation. Moreover, stiffness values determined for oriented single crystals of Fe(TPP)(2-MeHIm) and Fe(TPP)(2-$MeIm^-$) confirm that deprotonation of the axial imidazole ligand inverts the relative strengths of Fe coordination parallel and perpendicular to the plane of the porphyrin [31], consistent with reported structural differences.

A recent NRVS investigation [32] of the engineered protein Fe_BMb illustrates the usefulness of a model-independent measure for the coordination strength of the Fe. Site-directed mutations introduced a second nonheme Fe site in the heme pocket of Mb, creating a biosynthetic model for the two-iron catalytic site of nitric oxide reductase [33]. In this case, selective replacement with ^{57}Fe allowed independent monitoring of the vibrational properties of the heme and nonheme Fe atoms. The VDOS reported [32] for the heme Fe of the reduced protein strongly resembled that observed for deoxyMb (Fig. 2), resulting in a 182 ± 9 pN/pm value for the stiffness that is experimentally indistinguishable from the value determined for deoxyMb (Table 1). This indicates that the heme site is minimally perturbed by introduction of the second metal site, consistent with the reported crystallographic model for Fe_BMb [33].

In contrast, substitution of ^{57}Fe at the engineered nonheme site leads to observation of a distinct VDOS and confirms that vibrations of the heme and nonheme Fe atoms can be probed independently [32]. Although the nonheme Fe coordinates the same number of ligands (three histidine nitrogens, a glutamate oxygen, and a water oxygen), the 155 ± 6 pN/pm stiffness derived for the nonheme Fe reflects a slightly but significantly reduced coordination strength in comparison with that of the heme Fe (coordinated by five nitrogens

Table 2 Experimental stiffness values determined for iron porphyrins

	Stiffness (pN/pm)	Spin	Reference
(TPP)(2-MeHIm)	188 ± 1	2	[31]
Fe(TPP)(2-MeIm$^-$)	171 ± 5	2	[31]
Fe(P)(Cl)	192 ± 2	5/2	[30]
Fe(PPIX)(Cl)	197 ± 4	5/2	[30]

from the heme and from a histidine). This conclusion is possible even though individual Fe-ligand vibrations are not clearly resolved in the nonheme VDOS, presumable because of the lower symmetry of this site.

We anticipate that the stiffness will become a powerful quantitative probe for structural changes of metal sites in proteins. For example, the low spin heme resulting from coordination of NO or O_2 to native or mutant Mb exhibits stiffnesses in the $320 - 370$ pN/pm range [32, 34] that are significantly enhanced in comparison with those observed for deoxyMb (Table 1). Of course, the stiffness concept is not restricted to systems of biological interest, and recent use of the stiffness derived from ^{119}Sn NRVS measurements to quantify differences in the coordination of Sn in clathrate structures [35] illustrates its value in characterizing other complex structures.

Resilience Zaccai [36] introduced the concept of *resilience*

$$k_r = \frac{k_B}{d\left\langle x_j^2 \right\rangle / dT} \tag{3}$$

to quantify the temperature dependence of the atomic mean square displacement (MSD) for different proteins, as obtained with different techniques. Here, k_B is the Boltzmann constant. We note that k_r as defined by (3) is larger than that given in ref. [36] by a factor of three, corresponding to an average (rather than a sum) over the direction of motion.

Neutron scattering [36, 37] and Mössbauer [38, 39] measurements on various proteins revealed that MSD (of the hydrogens and iron, respectively) depend on temperature almost linearly up to ≈ 200 K, followed by a significant increase above the so-called dynamical transition temperature T_c. Traditionally, this sudden increase was interpreted as the result of the activation of protein-specific motions, which can be described as quasidiffusive motions within the molecule around the average structure, although recent studies [40, 41] argue that the increase in the MSD results from fluctuations in the protein's hydration shell.

The vibrational contribution to the resilience of the iron environment can be calculated directly from the Fe VDOS according to [42]

$$k_r = m_{Fe}\left\langle \omega^{-2} \right\rangle^{-1} = 3\frac{m_{Fe}\,(2\pi c)^2}{\int_0^\infty \bar{\nu}^{-2} D(\bar{\nu}) d\bar{\nu}}, \tag{4}$$

in which $\omega = 2\pi c\bar{\nu}$.

As seen from the lower traces in Fig. 2, modes below 100 cm^{-1}, which are thermally excited at physiological temperatures, make the dominant contribution to the resilience of the iron environment. Resilience values were found to be approximately 50 % higher for cyt *c* than for deoxyMb both experimentally (Table 1) and computationally [42]. Other experiments have also suggested reduced conformational flexibility for cyt *c*. Spectral diffusion of the heme-bound N-O stretching frequency on picosecond time scales is significantly slower

for cyt *c* than for myoglobin [43]. Large values of the order parameters for N-H bond and methyl group symmetry axis vectors determined from NMR measurements suggest that cyt *c* is less flexible than typical proteins on subnanosecond time scales [44].

These results confirm quantitatively the expectation that the resilience of the iron environment in cyt *c* is larger than in deoxyMb due to the additional linkages between the heme and the protein in the former, which restrict its mobility (3). A later study [45] further confirmed this expectation by identifying an even lower resilience for an iron porphyrin (Fe(OEP)(Cl) in Table 1) mimicking the protein heme but, evidently, with no covalent bonds to limit its mobility. Interestingly, neutron scattering data yielded a value of ≈ 8 pN/pm for the resilience of the hydrogen sites [36] in deoxyMb, indicating that motion of the heme site is more restricted than that of the hydrogens on average.

NRVS measurements on Fe_BMb [32] determined that the resilience of the heme Fe was unchanged with respect to native deoxyMb, indicating that incorporation of the second Fe site does not significantly perturb the structural dynamics. Moreover, it is particularly interesting to note that the resilience determined for both heme and nonheme irons in Fe_BMb is identical, within experimental uncertainty, in contrast with the lower stiffness determined for the nonheme site. This observation is not unexpected, since the frequencies below 100 cm^{-1} that dominate the experimental resilience (Fig. 2) reflect motion of the heme in response to global fluctuations of the protein [42]. This observation supports the expectation that the resilience measures the flexibility of the protein matrix in which the neighboring iron sites are embedded.

Contrasting stiffness and resilience The distinction between these force constants is somewhat academic for a hypothetical isotropic Debye solid with a normalized VDOS

$$D(\omega) = \begin{cases} 9\omega^2/\omega_D^3 & \omega < \omega_D \\ 0 & \omega > \omega_D \end{cases}, \tag{5}$$

for which integration shows that the stiffness $k_s = \frac{3}{5} m_j \omega_D^2$ and resilience $k_r = \frac{1}{3} m_j \omega_D^2$ differ by less than a factor 2. More significant differences are observed for real materials exhibiting a wider range of vibrational frequencies. In particular, the starker contrast between these effective force constants observed for biomolecules reflects the variation between relatively stiff covalent bonds and softer torsional degrees of freedom that is characteristic of these polymeric materials and, in fact, essential to their function.

The Appendix briefly sketches general analytical considerations for a harmonic system that clarify the distinction between stiffness and resilience. The stiffness k_s measures the force $F = -k_s x_j$ acting on atom j when it is displaced by a distance x_j, *with all other atoms fixed at their equilibrium positions*. As a result, the stiffness primarily probes nearest-neighbor interactions. In agreement with this interpretation, the results in Table 1 show a strong correlation between shorter Fe-ligand bonds and increased stiffness.

In contrast, the resilience k_r determines the displacement $x_j = F/k_r$ of atom j in response to an applied force F, *with the surrounding atoms free to respond*, but with the center of mass fixed. As a result, we expect that the resilience will reflect the elasticity of the surrounding material. The resilience also increases significantly as the number of covalent bonds between the heme and its environment increases for the (admittedly limited) range of measurements included in Table 1.

Measurements of a wider range of materials should further clarify the factors contributing to the measured resilience and enhance its value as a molecular probe. For example, the decrease in stiffness (by roughly 25 %) observed for $GeSb_2Te_4$ upon transition from an amorphous to a crystalline phase reflects the softening of the optical phonons [46]. It

seems likely that an experimental determination of the resilience using these NRVS data would quantitatively capture the observed hardening of the acoustic phonons upon the same transition.

The development in the Appendix indicates that both stiffness and resilience should properly be considered tensor quantities and, in general, will vary with orientation. However, measurements on frozen solutions or powders yield scalar values averaged over molecular orientation.

Compressibility As discussed above, resilience and stiffness probe the flexibility of the iron environment. In addition to that, NRVS can be used in combination with IXS to extract the compressibility of the whole protein, a quantity directly related to the protein structure (via its dependence on internal cavities, hydration, amino acid composition, etc.), dynamics (through its relation to the mean square displacement of atoms and volume fluctuations), and function (conformational changes). This method has been applied recently on Fe(III) cyt *c* [47]. Traditionally, this quantity has been determined from sound velocity measurements on dilute solutions at much lower frequencies, but the reported values vary considerably [48–51].

At low energies, the NRVS signal comes from collective motions of the entire molecule, rather than just from the Mössbauer isotope [52, 53]. This region of the NRVS spectrum yields the Debye sound velocity

$$v_D = \left(\frac{m_{Fe}}{2\pi^2 \rho \hbar^3} \frac{E^2}{D(E)} \right)^{\frac{1}{3}}, \tag{6}$$

where m_{Fe} is the mass of the iron atom and ρ is the protein mass density.

NRVS and IXS measurements yield v_D (6) and v_L (1), which allow one to calculate the transverse sound velocity v_T from

$$\frac{1}{v_D^3} = \frac{1}{3}\frac{1}{v_L^3} + \frac{2}{3}\frac{1}{v_T^3}, \tag{7}$$

and the bulk modulus (K_S = 12.3 GPa) and the compressibility (β_S = 0.08 GPa^{-1}) from

$$K_S = \frac{1}{\beta_S} = \rho \left(v_L^2 - \frac{4}{3} v_T^2 \right). \tag{8}$$

NRVS *and* IXS measurements on the same material are rare [54–56]. While cyt *c* is, to the best of our knowledge, the only material whose bulk modulus has been determined from a combination of these two techniques [47], insertion of published results from independent NRVS [54] and IXS [55] studies of metallic iron in (6)–(8) reproduces its well-known [57] elastic constants (Table 3).

Although this method seems to be applicable only to ^{57}Fe-enriched proteins, that is not necessarily true. In the low-energy region, the iron partial density of states coincides with the density of states of the hydrogens measured with (*incoherent*) inelastic neutron scattering (INS) [52] in the region below 10 cm^{-1}, which determines the averaged Debye velocity (6). (At higher energies, the hydrogen VDOS exhibits an excess relative to iron [52], which accounts for the lower resilience of the hydrogens [36].) In contrast, transverse acoustic modes make no contribution to the *coherent* scattering signal measured with IXS, which thus yields the velocity of the longitudinal acoustic modes (1). Therefore, for the purpose of

Table 3 Elastic constants extracted from IXS and NRVS measurements on iron and cytochrome *c*

Modulus (GPa)	Iron	Cyt *c*
$L = \rho v_L^2$	275	16
$G = \rho v_T^2$	79	3
$K_S = L - \frac{4}{3}G$	170	12.3

probing the protein globally, one could potentially combine the IXS results with those produced by INS measurements to determine the compressibility of biomolecular complexes that lack a useful NRVS probe nucleus.

Appendix: Stiffness and resilience of atoms in a harmonic system

In a harmonic system, the potential

$$V = \sum_{\alpha} \frac{1}{2} \omega_{\alpha}^2 Q_{\alpha}^2$$

takes a diagonal form in terms of normal coordinates

$$Q_{\alpha} = \sum_{j} \vec{e}_{j\alpha} \cdot \vec{r}_j m_j^{1/2}$$

connected to the mass-weighted Cartesian atomic displacement of atom j by the linear transformation coefficients

$$\vec{e}_{j\alpha} = m_j^{1/2} \frac{\partial \vec{r}}{\partial Q_{\alpha}} = m_j^{-1/2} \vec{\nabla}_j Q_{\alpha}.$$

The transformation is orthornormal, so that the same coefficients describe the inverse transformation

$$\vec{r}_j = \sum_{\alpha} Q_{\alpha} \vec{e}_{j\alpha} m_j^{-1/2}.$$

An atom j displaced from equilibrium experiences a restoring force

$$\vec{F} = -\vec{\nabla}_j V = -m_j^{1/2} \sum_{\alpha} \omega_{\alpha}^2 \vec{e}_{j\alpha} Q_{\alpha} = -m_j \left[\sum_{\alpha} \omega_{\alpha}^2 \vec{e}_{j\alpha} \vec{e}_{j\alpha} \right] \cdot \vec{r}_j$$

if all other atoms are fixed at their equilibrium positions. The *stiffness*

$$k_s = m_j \left\langle \omega^2 \right\rangle = \frac{1}{3} m_j \sum_{\alpha} \omega_{\alpha}^2 e_{j\alpha}^2 = \frac{1}{3} m_j \int \omega^2 D_j(\omega)\, d\omega$$

describes the restoring force $F = -k_s x_j$ averaged over all possible directions of displacement by a magnitude x_j.

In contrast, application of a force $\vec{F}$ to atom j adds a bias term to the harmonic potential. The minimum of the biased potential is displaced along each of the normal coordinates by an amount

$$Q_{\alpha} = \frac{1}{\omega_{\alpha}^2} \vec{F} \cdot \frac{\partial \vec{r}_j}{\partial Q_{\alpha}} = \frac{\vec{F} \cdot \vec{e}_{j\alpha}}{m_j^{1/2} \omega_{\alpha}^2},$$

resulting in a displacement $\vec{r}_k = \sum_\alpha Q_\alpha \vec{e}_{k\alpha}/m_k^{1/2}$ of the equilibrium position of each atom k. In particular, the equilibrium position of atom j shifts by an amount

$$\vec{r}_j = \vec{F} \cdot \sum_\alpha \frac{\vec{e}_{j\alpha}\vec{e}_{j\alpha}}{m_j \omega_\alpha^2}$$

proportional to the applied force. The resilience

$$k_r = m_j \left\langle \omega^{-2} \right\rangle^{-1} = \frac{3m_j}{\sum_\alpha e_{j\alpha}^2/\omega_\alpha^2} = \frac{3m_j}{\int \left(D_j\left(\omega\right)/\omega^2\right) d\omega}$$

describes the magnitude $x_j = F/k_r$ of this displacement averaged over all possible directions of the applied force.

References

1. Sage, J.T., Durbin, S.M., Sturhahn, W., Wharton, D.C., Champion, P.M., Hession, P., Sutter, J., Alp. E.E.: Long-range reactive dynamics in myoglobin. Phys. Rev Lett. **86**, 4966–4969 (2001)
2. Adams, K.L., Tsoi, S., Yan, J., Durbin, S.M., Ramdas, A.K., Cramer, W.A., Sturhahn, W., Alp, E.E., Schulz, C.: Fe vibrational spectroscopy of myoglobin and cytochrome f. J. Phys. Chem. B **110**, 530–536 (2006)
3. Zeng, W., Barabanschikov, A., Zhang, Y., Zhao, J., Sturhahn, W., Alp, E.E., Sage, J.T.: Synchrotron-derived vibrational data confirm unprotonated oxo ligand in myoglobin compound II. J. Am. Chem. Soc. **130**, 1816–1817 (2008)
4. Moeser, B., Janoschka, A., Wolny, J.A., Paulsen, H., Filippov, I., Berry, R.E., Zhang, H., Chumakov, A.I., Walker, F.A., Schünemann, V.: Nuclear inelastic scattering and Mössbauer spectroscopy as local probes for ligand binding modes and electronic properties in proteins: Vibrational behavior of a ferriheme center inside a β-barrel protein. J. Am. Chem. Soc. **134**, 4216–4228 (2012)
5. Xiao, Y., Wang, H., George, S.J., Smith, M.C., Adams, M.W.W., Jenney, F.E. Jr., Sturhahn, W., Alp, E.E., Zhao, J., Yoda, Y., Dey, A., Solomon, E.I., Cramer, S.P.: Normal mode analysis of Pyrococcus furiosus rubredoxin via nuclear resonance vibrational spectroscopy (NRVS) and resonance Raman spectroscopy. J. Am. Chem. Soc. **127**, 14596–14606 (2005)
6. Cramer, S.P., Xiao, Y., Wang, H., Guo, Y., Smith, M.C.: Nuclear resonance vibrational spectroscopy(NRVS) of Fe-S model compounds, Fe-S proteins, and nitrogenase. Hyperfine Interact. **170**, 47–54 (2006)
7. Tonzetich, Z.J., Wang, H., Mitra, D., Tinberg, C.E., Do, L.H., Jenney, F.E. Jr., Adams, M.W.W., Cramer, S.P., Lippard, S.J.: Identification of protein-bound dinitrosyl iron complexes by nuclear resonance vibrational spectroscopy. J. Am. Chem. Soc. **132**, 6914–6916 (2010)
8. Ogata, H., Krämer, T., Wang, H., Schilter, D., Pelmenschikov, V., van Gastel, M., Neese, F., Rauchfuss, T.B., Gee, L.B., Scott, A.D., Yoda, Y., Tanaka, Y., Lubitz, W., Cramer, S.P.: Hydride bridge in [NiFe]-hydrogenase observed by nuclear resonance vibrational spectroscopy. Nat. Commun. **6**, 7890 (2015)
9. Liu, L.V., Bell, C.B. III., Wong, S.D., Wilson, S.A., Kwak, Y., Chow, M.S., Zhao, J., Hodgson, K.O., Hedman, B., Solomon, E.I.: Definition of the intermediates and mechanism of the anticancer drug bleomycin using nuclear resonance vibrational spectroscopy and related methods. Proc. Natl. Acad. Sci. U. S. A. **107**, 22419–22424 (2010)
10. Bell, C.B. III., Wong, S.D., Xiao, Y., Klinker, E.J., Tenderholt, A.L., Smith, M.C., Rohde, J.-U., Que, L. J.r., Cramer, S.P., Solomon, E.I.: A combined NRVS and DFT study of Fe-IV=O model complexes: A diagnostic method for the elucidation of non-heme iron enzyme intermediates. Angew. Chem. Int. Ed. **47**, 9071–9074 (2008)
11. Wong, S.D., Srnec, M., Matthews, M.L., Liu, L.V., Kwak, Y., Park, K., Bell, C.B. III., Alp, E.E., Zhao, J., Yoda, Y., Kitao, S., Seto, M., Krebs, C., Bollinger, J.M. Jr., Solomon, E.I.: Elucidation of the Fe(IV)=O intermediate in the catalytic cycle of the halogenase SyrB2. Nature **499**, 320–323 (2013)
12. Green, M.T.: Application of Badger's rule to heme and non-heme iron-oxygen bonds: An examination of ferryl protonation states. J. Am. Chem. Soc. **128**, 1902–1906 (2006)
13. Suydam, I.T., Snow, C.D., Pande, V.S., Boxer, S.G.: Electric fields at the active site of an enzyme direct comparison of experiment with theory. Science **313**, 200–204 (2006)
14. Sturhahn, W.: Nuclear resonant spectroscopy. J. Phys.: Condens. Mat. **16**, S497–S530 (2004)

15. Sage, J.T., Paxson, C., Wyllie, G.R.A., Sturhahn, W., Durbin, S.M., Champion, P.M., Alp, E.E., Scheidt, W.R.: Nuclear resonance vibrational spectroscopy of a protein active-site mimic. J. Phys. Condens. Mat. **13**, 7707–7722 (2001)
16. Zeng, W., Silvernail, N.J., Scheidt, W.R., Sage, J.T.: Nuclear Resonance Vibrational Spectroscopy (NRVS). In: Scott, R.A., Lukehart, C.M. (eds.) Applications of Physical Methods to Inorganic and Bioinorganic Chemistry, pp. 401–421. Wiley, Chichester (2007)
17. Shenoy, G.: Basic characteristics of synchrotron radiation. Struct. Chem. **14**, 3–14 (2003)
18. Lipkin, H.J.: Mössbauer sum rules for use with synchrotron sources. Phys. Rev. B **52**, 10073–10079 (1995)
19. Sturhahn, W.: CONUSS and PHOENIX: Evaluation of nuclear resonant scattering data. Hyperfine Interact. **125**, 149–172 (2000)
20. Alp, E.E., Sturhahn, W., Toellner, T.S., Zhao, J., Hu, M., Brown, D.E.: Vibrational dynamics studies by nuclear resonant inelastic X-ray scattering. Hyperfine Interact. **145**, 3–20 (2002)
21. Burkel, E.: Phonon spectroscopy by inelastic X-ray spectroscopy. Rep. Prog. Phys. **63**, 171–232 (2000)
22. Sinn, H.: Spectroscopy with meV energy resolution. J. Phys.: Condens. Mat. **13**, 7525–7537 (2001)
23. Chen, S.H., Liao, C.Y., Huang, H.W., Weiss, T.M., Bellisent-Funel, M.C., Sette, F.: Collective dynamics in fully hydrated phospholipid bilayers studied by inelastical X-ray scattering. Phys. Rev Lett. **86**, 740–743 (2001)
24. Liu, Y., Chen, S.-H., Berti, D., Baglioni, P., Alatas, A., Sinn, H., Alp, E., Said, A.: Effects of counterion valency on the damping of phonons propagating along the axial direction of liquid-crystalline DNA. J. Chem. Phys. **123**, 214909 (2005)
25. Yoshida, K., Hosokawa, S., Baron, A.Q.R., Yamaguchi, T.: Collective dynamics of hydrated beta-lactogloblin by inelastic X-ray scattering. J. Chem. Phys. **133**, 134501 (2010)
26. Alatas, A., Leu, B.M., Zhao, J., Yavaş, H., Toellner, T.S., Alp, E.E.: Improved focusing capability for inelastic X-ray spectrometer at 3-ID of the APS:A combination of toroidal and Kirkpatrick-Baez (KB) mirrors. Nucl. Instrum. Meth. A **649**, 166–68 (2011)
27. Teale, F.W.J.: Cleavage of the haem-protein link by acid methylethylketone. Biochim. Biophys. Acta **35**, 543 (1959)
28. Leu, B.M., Ching, T., Tran, C., Sage, J.T.: Spectroscopic characterization of ^{57}Fe-enriched cytochrome *c*. Anal. Biochem. **423**, 129–132 (2012)
29. Leu, B.M., Ching, T.H., Zhao, J., Sturhahn, W., Alp, E.E., Sage, J.T.: Vibrational dynamics of iron in cytochrome *c*. J. Phys. Chem. B **113**, 2193–2200 (2009)
30. Barabanschikov, A., Demidov, A., Kubo, M., Champion, P.M., Sage, J.T., Zhao, J., Sturhahn, W., Alp, E.E.: Spectroscopic identification of reactive porphyrin motions. J. Chem. Phys. **135**, 015101 (2011)
31. Hu, C., Peng, Q., Silvernail, N.J., Barabanschikov, A., Zhao, J., Alp, E.E., Sturhahn, W., Sage, J.T., Scheidt, W.R.: Effects of imidazole deprotonation on vibrational spectra of high-spin iron(II) porphyrinates. Inorg. Chem. **52**, 3170–3177 (2013)
32. Chakraborty, S., Reed, J., Sage, J.T., Branagan, N.C., Petrik, I.D., Miner, K.D., Hu, M.Y., Zhao, J., Alp, E.E., Lu, Y.: Recent advances in biosynthetic modeling of nitric oxide reductases and insights gained from nuclear resonance vibrational and other spectroscopic studies. Inorg. Chem. **54**, 9317–9329 (2015)
33. Yeung, N., Lin, Y.-W., Gao, Y.-G., Zhao, X., Russell, B.S., Lei, L., Miner, K.D., Robinson, H., Lu, Y.: Rational design of a structural and functional nitric oxide reductase. Nature **462**, 1079–1082 (2009)
34. Zeng, W., Barabanschikov, A., Wang, N., Lu, Y., Zhao, J., Sturhahn, W., Alp, E.E., Sage, J.T.: Vibrational dynamics of oxygenated heme proteins. Chem. Commun. **48**, 6340–6342 (2012)
35. Leu, B.M., Sturza, M., Hu, M.Y., Gosztola, D., Baran, V., Fässler, T.F., Alp, E.E.: Vibrational dynamics of the host framework in Sn clathrates. Phys. Rev. B **90**, 104304 (2014)
36. Zaccai, G.: How soft is a protein? A protein dynamics force constant measured by neutron scattering. Science **288**, 1604–1607 (2000)
37. Doster, W., Cusack, S., Petry, W.: Dynamical transition of myoglobin revealed by inelastic neutron scattering. Nature **337**, 754–756 (1989)
38. Frolov, E.N., Gvosdev, R., Goldanskii, V.I., Parak, F.G.: Differences in the dynamics of oxidized and reduced cytochrome *c* measured by Mössbauer spectroscopy. J. Biol. Inorg. Chem. **2**, 710–713 (1997)
39. Parak, F.G.: Proteins in action: The physics of structural fluctuations and conformational changes. Curr. Opin. Struc. Biol. **13**, 552–557 (2003)
40. Young, R.D., Frauenfelder, H., Fenimore, P.W.: Mössbauer effect in proteins. Phys. Rev Lett. **107**, 158102 (2011)
41. Matyushov, D.V., Morozov, A.Y.: Electrostatics of the protein-water interface and the dynamical transition in proteins. Phys. Rev. E **84**, 011908 (2011)
42. Leu, B.M., Zhang, Y., Bu, L., Straub, J.E., Zhao, J., Sturhahn, W., Alp, E.E., Sage, J.T.: Resilience of the iron environment in heme proteins. Biophys. J. **95**, 5874–5889 (2008)

43. Hunt, N.T., Greetham, G.M., Towrie, M., Parker, A.W., Tucker, N.P.: Relationship between protein structural fluctuations and rebinding dynamics in ferric haem nitrosyls. Biochem. J. **433**, 459–468 (2011)
44. Liu, W., Rumbley, J.N., Englander, S.W., Wand, A.J.: Fast structural dynamics in reduced and oxidized cytochrome *c*. Protein Sci. **18**, 670–674 (2009)
45. Leu, B.M., Sage, J.T., Silvernail, N.J., Scheidt, W.R., Alatas, A., Alp, E.E., Sturhahn, W.: Bulk modulus of a protein active-site mimic. J. Phys. Chem. B **115**, 4469–4473 (2011)
46. Matsunaga, T., Yamada, N., Kojima, R., Shamoto, S., Sato, M., Tanida, H., Uruga, T., Kohara, S., Takata, M., Zalden, P., Bruns, G., Sergueev, I., Wille, H.C., Hermann, R.P., Wuttig, M.: Phase-change materials: Vibrational softening upon crystallization and its impact on thermal properties. Adv. Func. Mater. **21**, 2232–2239 (2011)
47. Leu, B.M., Alatas, A., Sinn, H., Alp, E.E., Said, A.H., Yavaş, H., Zhao, J., Sage, J.T., Sturhahn, W.: Protein elasticity probed with two synchrotron-based techniques. J. Phys. Chem. **132**, 085103 (2010)
48. Gekko, K., Hasegawa, Y.: Compressibility-structure relationship of globular proteins. Biochemistry **25**, 6563–6571 (1986)
49. Eden, D., Matthew, J.B., Rosa, J.J., Richards, F.M.: Increase in apparent compressibility of cytochrome c upon oxidation. Proc. Natl. Acad. Sci. U. S A. **79**, 815–819 (1982)
50. Chalikian, T.V., Totrov, M., Abagyan, R., Breslauer, K.J.: The hydration of globular proteins as derived from volume and compressibility measurements: Cross correlating thermodynamic and structural data. J. Mol. Biol. **260**, 588–603 (1996)
51. Valdez, D., Le Huérou, J.-Y., Gindre, M., Urbach, W., Waks, M.: Hydration and protein folding in water and in reverse micelles: Compressibility and volume changes. Biophys. J. **80**, 2751–2760 (2001)
52. Achterhold, K., Keppler, C., Ostermann, A., van Bürck, U., Sturhahn, W., Alp, E.E., Parak, F.G.: Vibrational dynamics of myoglobin determined by the phonon-assisted Mössbauer effect. Phys. Rev. E **65**, 051916 (2002)
53. Chumakov, A.I., Rüffer, R., Leupold, O., Sergueev, I.: Insight to dynamics of molecules with nuclear inelastic scattering. Struct. Chem. **14**, 109–119 (2003)
54. Shen, G., Sturhahn, W., Alp, E.E., Zhao, J., Toellner, T.S., Prakapenka, V.B., Meng, Y., Mao, H.-R.: Phonon density of states in iron at high pressures and high temperatures. Phys. Chem. Miner. **31**, 353–359 (2004)
55. Fiquet, G., Badro, J., Guyot, F., Requardt, H., Krisch, M.: Sound velocities in iron to 110 Gigapascals. Science **291**, 468–471 (2001)
56. Tsutsui, S., Kobayashi, H., Ishikawa, D., Sutter, J.P., Baron, A.Q.R., Hasegawa, T., Ogita, N., Udagawa, M., Yoda, Y., Onodera, H., Kikuchi, D., Sugawara, H., Sekine, C., Shirotani, I., Sato, H.: Direct observation of low-energy Sm phonon in $SmRu_4P_{12}$. J. Phys. Soc. Jpn. **77**, 033601 (2008)
57. Rayne, J.A., Chandrasekhar, B.S.: Elastic constants of iron from 4.2 to 300° K. Phys. Rev. B **122**, 1714–1716 (1961)